Experimental Thermal and Fluid Science 169 (2025) 111527

Contents lists available at ScienceDirect

Experimental Thermal and Fluid Science

journal homepage: www.elsevier.com/locate/etfs

Performance analysis of novel wavy-wall-based flow control method for wind turbine blade

Artur Dróżdż [a,*], Vasyl Sokolenko [a,b], Witold Elsner [a]

[a] Czestochowa University of Technology, Department of Thermal Machinery, Armii Krajowej 21, Czestochowa, 42-200, Poland
[b] Institute of Low Temperature and Structure Research, Okólna 2, Wrocław, 50-422, Poland

ARTICLE INFO

Dataset link: https://doi.org/10.18150/FTHEI6

Keywords:
Turbulent boundary layer
Adverse pressure gradient
Passive flow control

ABSTRACT

In this paper, the experimental study in flat-plate turbulent boundary layer (TBL) under various Reynolds number and adverse pressure gradient (APG) conditions was performed downstream of the wavy wall, which proved to be effective in delaying flow separation in Dróżdż et al. (2021). Three Reynolds numbers that reproduce the effect of slow changes in wind conditions on a large-scale pitch adjusted wind turbine (range of wind speed: $5-40$ m/s) and three pressure gradient evolutions that reproduce sudden changes in the relative inflow wind angle resulting from a rotation cycle and/or a blade torsional deflection cycle were analysed. The effect of Reynolds number was found to have a weak dependence on the performance of the method, since there was only about a 2% reduction in performance in the Reynolds number range studied, compared to the maximum efficiency of 15.5%. In contrast, for the maximum change in the pressure gradient, a decrease of 8.8% in the efficiency of the flow control method was reported. Assuming that a strong change in the pressure distribution occurs for at most a quarter of the blade deflection cycle, the rotor efficiency decreases by no more than 3.5%. Thus, the total efficiency of the method is not less than 10%. The results show that the chosen corrugation geometry works well under both nominal and off-design wind turbine rotor conditions. It was also shown that the method's efficiency in postponing flow separation can be evaluated by increasing or maintaining total momentum, quantified by the changes in momentum-loss thickness due to wavy wall.

1. Introduction

Most practically relevant wall-bounded flows have a high Reynolds number and are fully turbulent. They are also characterised by varying pressure gradients, where adverse pressure gradients can cause boundary layer detachment and significantly increase flow losses. For example, turbulent separation on the upper surface of an aircraft wing leads to a sharp increase in drag and a drop in lift. This issue also affects other devices, such as turbomachinery blades [1,2] or wind turbine blades [3–8]. This last application is particularly relevant due to the recent significant increase in the unit power of wind turbines, especially those installed offshore [9]. Hence, research on drag reduction has focused on methods that can delay turbulent separation with minimal surface geometry modification, such as vortex generators [10,11], which gives approximately 20% of the production growth, but only for small wind turbines. Vortex generators on a large 5 MW wind turbine blade are known to increase production by only 1% of the total power [12]. However, as power increases further, their efficiency becomes negative. This is in line with McMasters and Henderson [13] who pointed out that the use of roughness at high Reynolds numbers may have an opposite effect on aerodynamic efficiency. As suggested in the review paper of Ricco et al. [14], even up to 15% of total drag reduction can be achieved by introducing effective separation control technologies using surface modification in aerodynamic systems, there have been several other proposals, such as the use of dimples [15–20] or grooves on blades [21], slotted airfoils [22,23], microcylinder near the leading edge of the blade [7,24,25]. However, as the effectiveness of passive methods, due to the predominance of turbulent boundary layers diminishes for high Reynolds number, it seems that the flow control is not possible without using actuators, which requires complex modification of the component structure and in addition, they are expensive in terms of external power supply.

One of the newer proposals of the passive method to reduce the risk of turbulent detachment at high Reynolds numbers is the use of a streamwise wavy wall (WW). In the experimental work of Dróżdż et al. [26], the authors demonstrated the possibility of increasing local wall shear stress and consequently postponing turbulent separation. The method has been proposed for the very first time by Dróżdż et al. [27]. The authors investigated an effect of waviness for a constant

* Corresponding author.
E-mail address: artur.drozdz@pcz.pl (A. Dróżdż).

https://doi.org/10.1016/j.expthermflusci.2025.111527
Received 20 January 2025; Received in revised form 26 March 2025; Accepted 15 May 2025
Available online 1 June 2025

amplitude to period ranging from 0.015 to 0.04 on skin friction (measured by oil film interferometry 240 mm downstream of the corrugated surface) under APG conditions and compared the results with the reference case in which TBL was developing on the flat plate. The experiment was performed for the Reynolds number $Re_\tau \approx 3300$. A huge growth of 13% in skin friction was observed for $A/\lambda = 0.0335$ (where A is the amplitude and λ is the period of waviness) which was accompanied by a significant increase in mean velocity in the inner region. Consequently, a significant delay in flow separation was achieved for the first time using wall surface modification at such a high Reynolds number. In a more recent experiment [26] the authors examined the performance of a wavy surface with a fixed streamwise viscous scaled amplitude $A^+ = Au_\tau/\nu$ (where the u_τ distribution is taken for the case with the flat wall) for a higher $Re_\tau \approx 4000$ and a similar effect on skin friction and, consequently, the postponement of flow separation has been observed. The 15% increase in skin friction was achieved, which is the highest documented in the literature so far due to the streamwise-orientated wavy wall. This approach can postpone TBL separation by approximately one boundary layer thickness, making it a strong candidate for practical implementation.

However, Elsner et al. [28]conducted a numerical analysis of the impact of the two-dimensional wavy wall on wall shear stress, using large-eddy simulation (LES), for a lower Reynolds number $Re_\tau \approx 1400$, for a lower Reynolds number. The LES results were experimentally verified. For this particular value Re_τ, the modified surface topology was found to not provide an increase in the wall shear stress downstream of the corrugation compared to the flat surface. This suggests that below a certain value of Re_τ the wavy wall becomes ineffective in postponing separation. Later, the investigations using numerical simulation performed by Kamiński et al. [29] about twice higher $Re_\tau \approx 2500$ confirmed beneficial impact on the wall normal velocity gradient and consequently on the wall shear stress, both along the wavy wall and, what is more important, in the region further downstream. Then, it was confirmed that the effect of the wavy wall can be attributed to a significant increase in the wall-normal velocity gradient. Dróżdż et al. [26] show that the amplified velocity fluctuations downstream of the wavy wall result from increased momentum transport to the wall from the outer layer and the dominant presence of small-scale sweeping motion. It can be clearly concluded that the presence of waviness crests affects turbulent structures, i.e sweep events similarly to high-speed large-scale regions created at high Reynolds numbers due to the amplitude modulation mechanism found by Mathis et al. [30]. The mean flows in the APG region is affected by this mechanism and thus the separation location, as shown in the model proposed by Dróżdż et al. [31]. In particular, the authors demonstrated that the viscous-scaled mean convection velocity U_C^+ in the inner region of the TBL is universal in APG flows, despite the decreasing mean velocity U^+. They identified that this behaviour is due to enhanced amplitude modulation, particularly an increase in the mean convection velocity of small-scale turbulence. It is particularly important that, as Liu et al. [32] pointed out, the strong correlation between instantaneous convection velocity of enstrophy and skin friction occurs in turbulent flow. In fact, small-scale vortices from high-speed regions exhibit increased sweeping motion due to faster convection velocity, delivering momentum when falling into low-speed regions. The increase in convection velocity in the APG flow was also reported in Ref. [33] using hot-wire anemometry and PIV methods. This process results in three inflection points on the high-deficit mean velocity profile [31]. In the case of the wavy wall, it induces high-speed regions on crests where small-scale turbulence originates and sheds downstream into troughs, delivering momentum by sweeping motion analogous to the amplitude modulation mechanism.

It is important to note how the wavy wall needs to be designed. Preliminary analyses indicate that the undulation should be located in the area where the Rotta-Clauser pressure gradient parameter $\beta = (\delta^*/\tau_w)\cdot(dP_e/dx)$ (where δ^* is the displacement thickness and dP_e/dx the streamwise pressure gradient in the freestream) do not exceed the value of 10. As indicated in Ref. [26], streamwise variation in amplitude should ensure that the amplitude $A^+ = 170$ is maintained, while the period should be adjusted in such a way that the flow in the troughs is kept on the verge of separation (which occurs when the effective slope is at the upper limit of the waviness regime ≈0.15). For lower amplitudes of the wavy wall, the beneficial effect diminishes. In contrast, too high an amplitude results in an extensive separation bubble in the troughs, causing the turbulence convection to equal the mean flow velocity. This makes the wavy wall mechanism inefficient in delivering momentum through small-scale sweeping motion.

It should be noted here that the streamwise distribution of WW amplitude strongly depends on the pressure gradient. Therefore, the efficient geometry of the corrugation should be dictated by the nominal/on-design flow conditions encountered in practical applications. One potential application of this method is the pitch-regulated wind turbine blade. The angle of attack (AoA) of the blade airfoil ranges from 3° to 8° [34], depending on the wind conditions. As the relative wind speed increases (range of wind speed: 10–40 m/s) the AoA is reduced to maintain a constant rotational speed and has a minimal effect on the change in the pressure gradient but some effect on Reynolds number. However, pressure gradient flow conditions can vary significantly when considering the variation at different rotational positions of the blade. In addition, the torsional deflection of the large-scale wind turbine blade rapidly alters the AoA and, therefore, the distribution of the pressure gradient.

The motivation for this work stems from the aforementioned variation in wind speed and inflow angle on large-scale wind turbine blades. Therefore, the first aim is to determine the universality of the wavy wall geometry selected in Ref. [26] within a certain range of changes in Reynolds number (slow changes in wind speed). The second aim is to determine the performance under unstable flow conditions at a constant Reynolds number, due to different rotational positions or torsional deflections (sudden changes in the flow inflow angle) causing temporal changes in the pressure gradient.

In the present paper, it was decided to rely both on the published and cited data [28,29,35], as well as on new results from a measurement campaign carried out downstream of the wavy wall for three different Reynolds numbers ($Re_\tau \approx 2600$, 4000 and 4500). The additional study was performed for the same WW geometry as in Ref. [26] but considering two weaker evolutions of APG. In addition, the percentage increase in the skin friction coefficient downstream of the wavy wall was calculated.

2. Experimental setup

The experiment was carried out in a wind tunnel at Czestochowa University of Technology where the TBL was developing along a 5035 mm long flat plate allowing the TBL to develop well just before the APG section, that is, at $x = 0$ (see Fig. 1). The two-dimensional WW section, where the waviness was extruded along the spanwise direction, has a total length of $L = 0.666$ m (5 periods streamwise with $\lambda \approx 0.133$ m). The amplitude of WW $A(x)$ increases downstream of the flow corresponding to the relation: $A(x) = (0.00366x^2 + 0.000614x + 0.003351)$ m. It is important to note that it is the same WW geometry as the optimal one from Ref. [26] (i.e. ensuring the highest growth in τ_w for $Re_\tau \approx 4000$).

The experiment was carried out for the value of the inlet velocity $U_{e,in} \approx 15, 24$ and 29 m/s, which corresponds to $Re_\tau \approx 2600$, 4000, and 4500. In each case, the measurements were taken downstream of the wavy surface and compared with the measurements without wavy surface. Detailed flow data in the inlet plane are shown in Table 1. The mean velocity and its fluctuation profiles were measured with a single hot-wire probe downstream of the wavy wall. The friction velocity values $u_\tau = \sqrt{\tau_w/\rho}$ (where $\tau_w = \mu dU/dy$ and μ is the dynamic viscosity and dU/dy is the velocity gradient at the wall) were estimated using the approach proposed by Niegodajew et al. [36]. The uncertainty of

Table 1
Inlet TBL parameters.

Symbol	$U_{e,in}$	δ_{in}	$Re_{\theta,in}$	$Re_{\tau,in}$	$C_{f,in}$	δ^*_{in}	θ_{in}	H_{in}	$u_{\tau,in}$
○	15	82.0	9177	2584	0.0025	14.1	10.2	1.38	0.51
◇, ◁, ▽	24	77.8	14 187	3732	0.0023	13.5	9.9	1.36	0.79
□	29	76.7	16 382	4479	0.0023	12.3	9.1	1.35	0.97

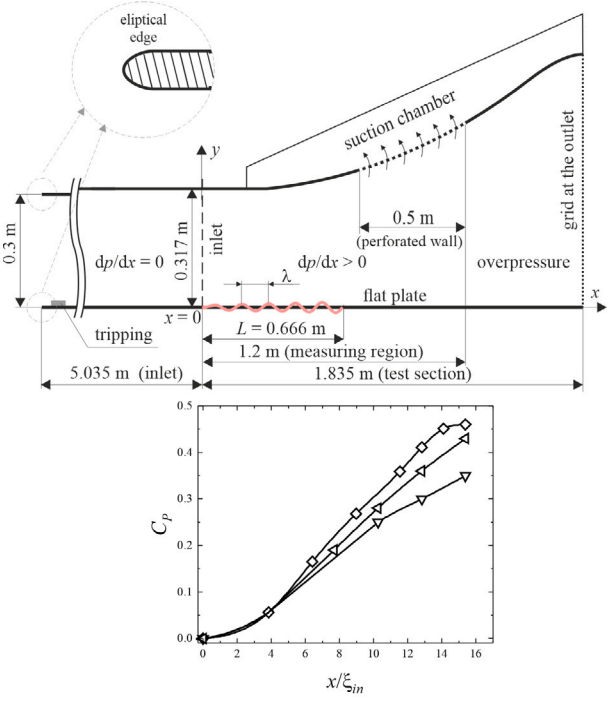

Fig. 1. Schematic of the test section and C_p distributions in measuring region.

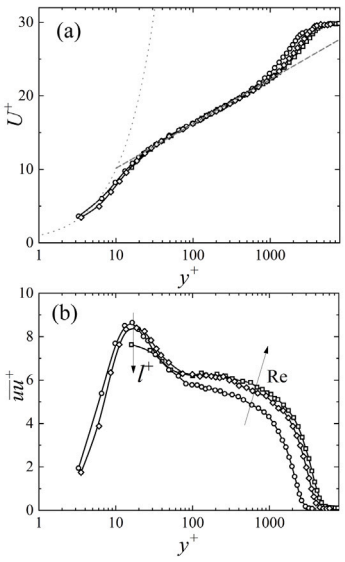

Fig. 2. Mean velocity (a) and turbulence intensity (b) profiles presented in viscous scale at $x = 0$. The dashed line represents the logarithmic law (with $\kappa = 0.38$ and $B = 4.1$) while the dotted line represents $y^+ = U^+$.

the friction velocity, verified against the oil film interferometry, was up to 2.5% for profiles characterised by $H < 2.0$ and up to 5.0% for $H > 2.0$. The uncertainties in the measurement/estimation of U and H were below the level of $0.01U_{in}$ and 1.5%, respectively.

A more detailed description of the experimental setup, including information about measurement uncertainties, can be found in our previous work [35]. The distributions of the pressure coefficient $C_P = 1 - (U_e/U_{e,in})^2$ in Fig. 1 were obtained by applying different suction conditions on the perforated upper wall (with 10% perforation of the surface area with 0.5 mm holes). It should be emphasised that the waviness, due to its low amplitude in relation to the height of the channel, does not affect the pressure distribution. The freestream velocity, and the pressure in the suction chamber were monitored with uncertainties levels 1% and 2.5% respectively.

3. Inlet conditions

Table 1 contains inlet data for three inflow velocities. For each case a symbol has been assigned, which we will use throughout the paper, and so, respectively, (○) refers to $Re_\tau \approx 2600$, (◇, ◁, ▽) $Re_\tau \approx 4000$, (□) $Re_\tau \approx 4500$. It can be seen that the thickness of the boundary layer decreases as a function of the Reynolds number, while an increase in friction velocity u_τ is observed. Fig. 2 shows the inlet profiles ($x/\delta = 0.0$ mm) of the mean velocity (Fig. 2(a)) and the streamwise Reynolds stresses in the viscous units (Fig. 2(b)), measured for the reference case (with a flat bottom wall). The Fig. 2(a) shows canonical zero pressure gradient behaviour of the flow at the inlet while Fig. 2(b) shows that $\overline{uu}$ increases with Reynolds number; however, it is observed in the outer region only since the length of the hot wire l^+ does not exceed the recommended value of 20 only for the lowest case Re_τ. The velocity profiles are measured using a sufficiently short length of wire to avoid small-scale energy attenuation, both in the inner and outer regions of the APG TBL, as recently observed in [37].

4. Results

4.1. Assessment of the effect of reynolds number on method performance

Assessment of the effect of Reynolds number on the proposed flow control method performance allows us to verify whether the effect (postponement of separation) is maintained for a certain range of Reynolds numbers. The amplitude of the surface undulations varies from $A^+ \approx 110$, $A^+ \approx 170$ and to $A^+ \approx 200$, respectively, for $Re_\tau \approx 2600$, $Re_\tau \approx 4000$, and $Re_\tau \approx 4500$. For the highest Re_τ, the waviness amplitude exceeds the lower bound of the logarithmic layer ($y^+ = 150$) of TBL (see Fig. 2 for reference). Please note that from Ref. [28] at $Re_\tau < 1400$ any wavy wall configuration was found to be effective in increasing skin friction. As the amplitude should be adjusted to the thickness of the inner region, which exceeds 15% of δ in this case the WW generates a large pressure drag that causes a decrease in skin friction downstream of the WW. Therefore, the mechanism of the increase in sweep events is too weak to counteract pressure-drag-induced skin friction loss. We therefore assumed that $Re_\tau \approx 1400$ is the limit of performance of the wavy wall since the two opposing effects, namely the pressure-drag-induced C_f loss from one side and the sweeping motion C_f gain from another side, are at a similar level.

The Fig. 3 shows the effect of the wavy wall (red area) on the C_f distributions acquired downstream for three cases $U_{e,in} \approx 15$ m/s ($Re_\tau \approx 2600$), reported previously in LES results in Ref. [29] ($Re_\tau \approx 2500$) (a), 24 m/s ($Re_\tau \approx 4000$), previously reported in experimental results in Ref. [35] b) and new results at 29 m/s ($Re_\tau \approx 4500$) (c) that correspond to (Fig. 3(a)), (Fig. 3(b)) and (Fig. 3(c)), respectively. The C_f for the wavy surface (open symbols) is compared with the C_f flat plate (dark

Table 2
Integrated C_f difference.

Symbol	Re_τ	Integration length [m]	Δx_s [m]	$\Delta x_s/\delta_{in}$ [–]	ΔC_f [–]	$\Delta C_f/C_{f,in}$ [%]
○	2600	0.667–1.14	0.13	1.2	0.000335	13.5%
◇	4000	0.667–1.34	0.19	2.5	0.000348	15.5%
□	4500	0.667–1.29	0.17	2.0	0.000318	14.1%

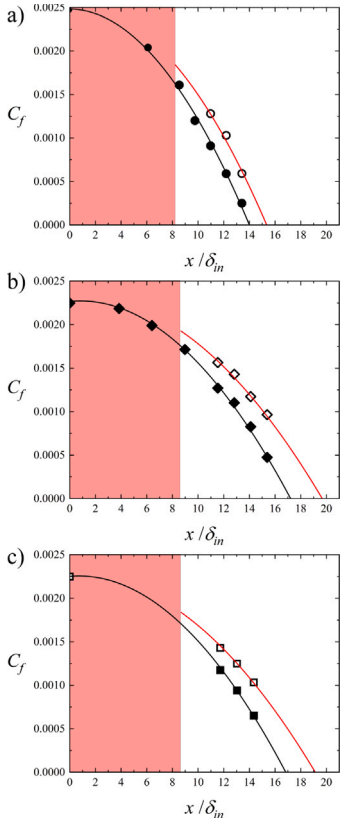

Fig. 3. Comparison of skin-friction coefficient distributions ($Re_\tau \approx 2600$ (a), ○, 4000 (b), ◇, 4500 □ (c)). The open symbol corresponds to the wavy wall while dark symbols corresponds to the flat plate.

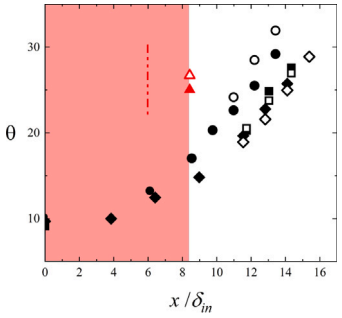

Fig. 4. Comparison of momentum loss thickness distributions ($Re_\tau \approx 2600$ (○), 4000 (◇), 4500 (□)). Open symbol is marked as wavy wall case while dark symbols corresponds to the flat plate. Red triangles corresponds to data at $Re_\tau \approx 900$ from Ref. [28], while red dashed-dotted line corresponds to the end of wavy wall for that case according to limit of $\beta < 10$.

symbols), where the distributions were extrapolated by a second-order polynomial to predict the separation point. The streamwise distance x was reduced by δ_{in}.

For lower $Re_\tau \approx 2600$ (Fig. 3(a)), we observe a weaker increase in C_f and a smaller postponement of flow separation of $\Delta x_s/\delta_{in} \approx 1.2$ when confronted with $Re_\tau \approx 4000$ where $\Delta x_s/\delta_{in} \approx 2.5$. This effect is due to lower amplitude than the thickness of the inner layer for that Reynolds number. When the Reynolds number increases to $Re_\tau \approx 4500$ (see Fig. 3(c)), the waviness-induced effect weakens, the postponement of the flow separation point at the level of $\Delta x_s/\delta_{in} \approx 2.0$. In this case, the thickness of the inner region is only slightly lower than that observed for $Re_\tau \approx 4000$.

For a more statistically confident estimate of the effect of waviness on the skin friction coefficient, the differences between the two distributions C_f were integrated from the end of the wavy wall to the flow separation location occurring for the flow without wall surface modification. This means that the integration length does not account for the separation shift Δx_s. Since the inlet value of $C_{f,in}$ decreases with the Reynolds number, the percentage value of ΔC_f was scaled by $C_{f,in}$ to assess the real effectiveness of the method.

The data in Table 2 show that the corrugation geometry selected according to the assumptions described above (referred to as the optimum geometry) produces the highest gain of 15.5%. For smaller and larger Reynolds numbers, the efficiency of the method decreases, but this change, within the range of Reynolds numbers analysed, is not significant and does not exceed 2%.However, the conclusions drawn from the analysis of the shift of the separation point and the increase C_f are consistent.

The skin friction coefficient indicates an increased strain rate at the wall, which should also translate into a momentum increase, but only near the wall. This raises the question: Does this come at the expense of reducing the momentum in the outer layer? An efficient method for postponing separation should be characterised by an increase or at least maintenance of the total momentum, not only by a momentum transfer towards the wall. To quantify the total momentum, the momentum loss thickness (θ) can be used. In Fig. 4, the distributions of θ as a function of x/δ_{in} for the wavy surface (open symbols) are compared with the distributions of θ as a function of x/δ_{in} on the flat plate (dark symbols). Symbols as in Table 1.

The results indicate an increase in momentum for the two highest Reynolds numbers, while only for $Re_\tau \approx 2600$ a decrease in total momentum is observed. This suggests that the lower amplitude relative to the inner region ($A^+ = 110$) results in a lower efficiency of the method for this particular Reynolds number. A similar effect is observed for the even lower Reynolds number $Re_\tau \approx 1400$ reported in Ref. [28], where both two- and three-dimensional geometry were considered, also changing the value of A^+ and the length of the corrugation. The length of the WW in the study corresponds to the red dashed-dotted line plotted in Fig. 4. For that both lower Reynolds numbers (red triangles and black dots) an increase in the momentum loss thickness is observed, which translates to a weaker transport of momentum to the wall by waviness. However, for $Re_\tau \approx 2600$ a properly adjusted amplitude of waviness that meets the requirement of $A^+ \approx 170$ should bring an increase in total momentum. The efficiency of WW can also be evaluated via the changes of Re_θ. The values of Re_θ as well as other important TBL parameters of 26 velocity profiles determined in APG region are shown in Table 3. It can be concluded that the optimal configuration causes the local Re_θ to decrease when using a wavy wall. The decreased Re_θ indicates the lower loss of momentum and the weaker effect on flow separation.

In order to gain a more detailed insight into the flow field modified by the wavy wall, the profiles of mean velocity and streamwise Reynolds stress downstream the flow for each Reynolds number are shown in Fig. 5. Note that the profiles are normalised by the edge

Table 3
Experimental TBL parameters for flat and wavy surfaces at different Reynolds number.

x/δ_{in}	x	U_e	δ	Re_θ	Re_τ	C_f	δ^*	θ	H	u_τ
Flat (15 m/s) in Ref. [35]										
6.10	0.50	13.5	99.2	11 485	2744	0.0020	19.50	13.24	1.47	0.43
8.54	0.70	12.5	116.6	13 737	2669	0.00161	27.60	17.03	1.62	0.36
9.76	0.80	12.0	131.0	15 794	2495	0.00120	36.20	20.31	1.78	0.30
10.98	0.90	11.6	142.5	16 979	2441	0.00091	44.70	22.63	1.97	0.25
12.20	1.00	11.3	158.4	18 975	2046	0.00059	56.80	25.50	2.23	0.20
13.41	1.10	10.9	185.2	20 458	1512	0.00027	76.6	29.19	2.62	0.13
Wavy (15 m/s)										
10.98	0.90	11.6	152.7	17 680	2760	0.00128	42.90	24.15	1.77	0.30
12.20	1.00	11.2	171.0	19 979	2674	0.00102	55.90	28.49	1.96	0.26
13.41	1.10	10.9	193.1	21 855	2166	0.00064	71.40	31.93	2.24	0.20
Flat (24 m/s) in Ref. [35]										
3.85	0.30	23.2	81.8	14 879	4074	0.00219	13.55	9.99	1.36	0.77
6.41	0.50	21.9	92.8	17 665	4283	0.00199	17.59	12.45	1.41	0.69
8.97	0.70	20.5	106.1	19 801	4155	0.00171	22.35	14.81	1.51	0.60
11.54	0.90	18.9	128.7	24 424	4033	0.00127	33.09	19.65	1.68	0.48
12.82	1.00	18.3	145.2	26 352	3937	0.00110	41.46	22.76	1.82	0.43
14.10	1.10	17.5	160.8	28 836	3931	0.00083	52.40	25.71	2.04	0.36
15.38	1.20	17.2	183.2	30 983	3656	0.0005	68.84	28.87	2.38	0.27
Wavy (24 m/s) in Ref. [26]										
11.54	0.90	19.0	121.6	22 722	4084	0.00156	29.95	18.92	1.58	0.54
12.82	1.00	18.4	132.8	25 078	4124	0.00143	36.38	21.58	1.69	0.50
14.10	1.10	17.7	149.6	27 431	3985	0.00117	47.03	24.95	1.89	0.43
15.38	1.20	17.2	170.1	30 933	4003	0.00097	59.35	28.87	2.06	0.38
Flat (29 m/s)										
11.73	0.90	23.0	131.7	28 833	4479	0.00117	34.41	20.27	1.70	0.56
13.04	1.00	21.7	154.6	33 724	4500	0.00092	49.09	24.84	1.98	0.47
14.34	1.10	21.6	169.5	37 035	4242	0.00062	61.52	27.58	2.23	0.39
Wavy (29 m/s)										
11.73	0.90	23.0	130.4	29 104	4944	0.00143	32.94	20.51	1.61	0.61
13.04	1.00	22.0	145.7	32 434	4970	0.00125	40.76	23.75	1.72	0.55
14.34	1.10	21.3	163.6	35 217	4857	0.00103	49.68	26.95	1.84	0.48

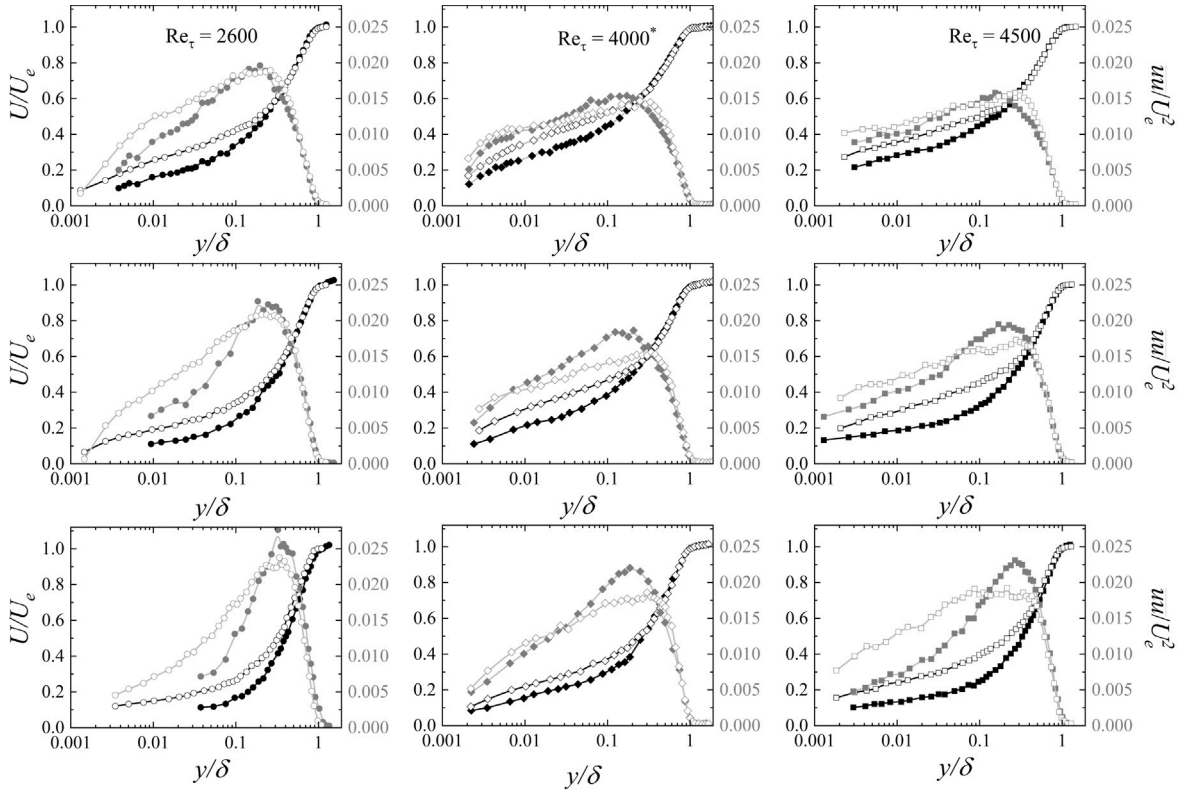

Fig. 5. Comparison of the mean velocity and velocity variance components: top row $x = 0.9$ m, middle row $x = 1.0$ m and bottom row $x = 1.1$ m. The star (*) indicates on-design conditions — the best adjustment of the wavy wall to flow conditions ($A^+ \approx 170$).

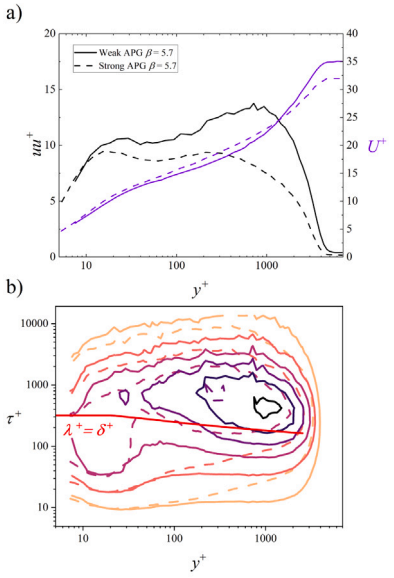

Fig. 6. Effect of flow history on Reynolds stresses for $\beta \approx 5.7$ for weak APG evolution ($x = 1.0$ m) - black contours and strong APG evolution - ($x = 0.5$ m) dashed contours (a) and premultiplied spectra E/u_τ^2 (b). The red line corresponds to streamwise spatial scale $\lambda^+ = 4000$. Increments marked by colours between iso-contour levels equals 0.4.

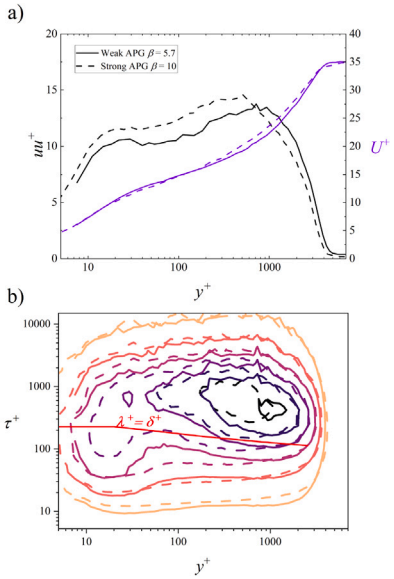

Fig. 7. Effect of flow history on Reynolds stresses for weak APG evolution $\beta \approx 5.7$ ($x = 1.0$ m) - black contours and $\beta \approx 10$ ($x = 0.7$ m) for strong APG evolution - dashed contours (a) and premultiplied spectra E/u_τ^2 (b). The red line corresponds to streamwise spatial scale $\lambda^+ = 4000$. Increments marked by colours between iso-contour levels equals 0.5.

velocity U_e and the streamwise evolution of these profiles is shown in subsequent rows ($x = 0.9$ m, 1.0 m, and 1.1 m). The black symbols correspond to the flat plate case, while the open symbols represent the profiles for the WW case.

All mean velocity profiles (obtained on the flat plate and those measured in the presence of wall undulations) collapse in the outer region for all Reynolds number cases, while in the inner part a notable increase in mean velocity caused by the waviness is observed. As can be seen, this increase in velocity hardly depends on the Reynolds number. The influence of Re can only be noticed by analysing the Reynolds stress profiles, especially for the $x = 1.0$ and 1.1 m traverses. In general, for the reference case, there is a decreasing outer peak value of $\overline{uu}/U_e^2$ with the Reynolds number. A direct comparison between profiles indicates that the wavy surface is responsible for flattening the outer maximum. The flattening rate increases with increasing x. There is also a noticeable increase in Reynolds stress distributions in the near-wall region. This effect can be attributed to the change in the flow history of the pressure gradient, as the distribution β is weaker for a wavy wall, causing the outer maximum to shift away from the wall.

4.2. Assessment of the effect of pressure gradient variation on method performance

This section focusses on sensitivity analysis, with the aim of examining the effect of different pressure gradient distributions on the performance of the wavy wall at a constant Reynolds number defined at the entrance to the APG section $Re_\tau \approx 4000$. Various suctions of the upper wall were applied in the APG section to obtain different pressure gradient distributions (see Fig. 1). The weak evolution of APG was achieved by completely sealing off the perforated upper wall.

Under varying pressure gradient conditions, the location of the ending wavy wall is $\beta \approx 10$, as established in Ref. [26] for strong APG conditions, and it moves to a lower β for weaker pressure gradient conditions. This raises the question of how it impacts the performance of the method. It should be noted that Vinuesa et al. [38] demonstrated that the flow history of the pressure gradient affects the specific state of the boundary layer for the same β. This factor is known to influence the location and strength of the outer maximum in Reynolds stress profiles [39]. Therefore, understanding these effects is crucial to optimising the design and performance of flow control methods applicable to APG flows.

To quantify the changes in turbulent energy levels due to the flow history of the APG, the mean velocity and Reynolds stress profiles (Fig. 6(a)) and iso-contours of the wavelet energy spectra E (equivalent to the premultiplied energy spectra) (Fig. 6(b)) are presented for the same value of $\beta \approx 5.7$ and two selected cases i.e. strong APG and weak APG. The reduced wavelet energy spectra E/u_τ^2 is presented as a function of the normalised time scale τ^+ and normalised wall distance y^+. As shown in Ref. [31], the mean convection velocity profile $U_C^+ = f(y^+)$ is universal in the inner region of TBLs, therefore, the spatial scale $\lambda^+ = 4000$ (red line) estimated using U_C^+ splits the spectra into small and large scales (values of τ^+ below and above that line), respectively.

The results presented in Fig. 6a show that the inner peak is generally universal for both cases, with an increase in the outer peak for a weak APG evolution. A more in-depth interpretation of the impact of flow history is possible by analysing the energy spectra in Fig. 6b. It reveals that the small-scale energy is universal at the inner peak, while at the outer peak, a significant growth of energy at all scales, but especially for the large scales, occurs. These results confirm that for the weaker evolution of APG, the large-scale contribution to flow dynamics increases faster with β. This leads to a stronger modulation of the small scales, while the small scales contribute less to the flow dynamics.

In Fig. 7, the flow structure for $\beta \approx 5.7$ occurring for weak APG evolution is compared to the flow structures for $\beta \approx 10$ occurring for strong APG evolution. The flow picture appears to be similar for both cases in Fig. 7. Therefore, termination the WW before $\beta \approx 5.7$ in case of weak APG evolution suffices. Extending it to $\beta \approx 10$ provides minimal benefits and may reduce the efficiency of the WW mechanism for increasing sweep events, potentially resulting in a reduced momentum. As $\beta \approx 5.7$ for weak APG evolution falls within $x = 1.0$ m from the inlet, this implies that keeping the same length of the wavy wall (0.666 m) still ensures high performance of the method, regardless of the evolution of the APG.

Another factor that impacts the performance of WW for different APGs is the amplitude of the wavy wall. For a strong APG evolution, the

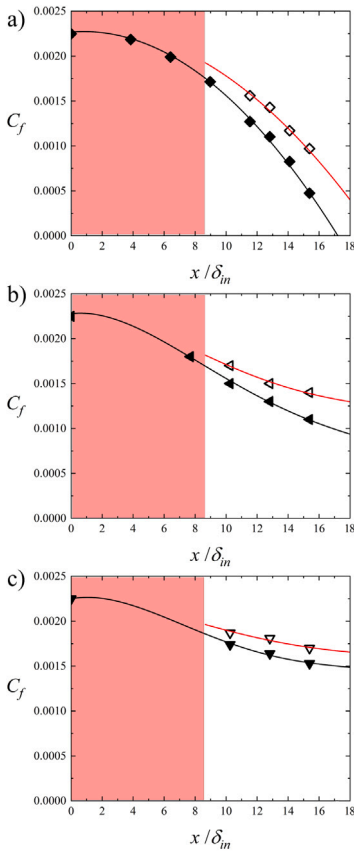

Fig. 8. Comparison of skin-friction coefficient distributions: strong APG (◊) a); moderate APG (◁) b) and weak APG (▽) c). The open symbol corresponds to the wavy wall while dark symbols corresponds to flat-plate.

Table 4
Integrated C_f difference - pressure gradient effect.

Symbol	*APG*	Re_τ	Integration length [m]	ΔC_f	$\Delta C_f/C_{f,in}$
◊	Strong	4000	0.667–1.34	0.000348	15.5%
◁	Moderate	4000	0.667–1.34	0.000203	10.2%
▽	Weak	4000	0.667–1.34	0.000150	6.7%

viscous-scaled amplitude A^+ is constant, but for two weaker APG evolutions it increases in A^+ and exceeds the thickness of the inner layer at the end of WW. The values of A^+ are 205 and 240 for moderately strong and weak APG evolutions, respectively.

The Fig. 8 shows the effect of the wavy wall (red area) on the C_f distributions downstream of the WW for $Re_\tau \approx 4000$ with strong APG (original conditions) (Fig. 3(a), moderately strong APG (Fig. 3(b) and weak APG (Fig. 3(c) evolutions. The C_f for the wavy surface (open symbols) is compared with the C_f for the flat plate (dark symbols). Distributions were extrapolated using a second-order polynomial for strong APG evolution and a fourth-order polynomial for moderately strong and weak APG evolutions. However, predicting the separation point was not possible because the test section was too short. The streamwise distance x was normalised by δ_{in}. Due to a slower decrease in friction velocity for weaker APG evolutions, the increase in C_f due to the wavy wall is weaker. This is expected because the amplitude rises in viscous units.

Similarly to the Re-effect, to evaluate the statistical effect of corrugation, the differences between the two C_f distributions were integrated from the end of the wavy wall to the flow separation location occurring for the flow without wall surface modification for strong APG evolution. The same integration length was applied for all evolutions

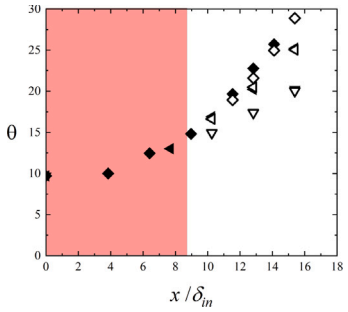

Fig. 9. Comparison of momentum loss thickness distributions: strong APG (◊), moderate APG (◁) and weak APG (▽). The open symbol corresponds to the wavy wall while dark symbols corresponds to flat-plate.

of pressure gradients. The integrated ΔC_f values were normalised by the $C_{f,in}$ value.

The data in Table 4 show that the selected corrugation geometry (referred to as the optimal geometry) produces an increase of 10.2% and 6.7% for moderately strong and weak APG evolutions, respectively. In these cases, the impact on WW performance is significant compared to the Reynolds number effect. Relating the obtained results to their practical application, such as for wind turbine blades, it should be remembered that strong changes in pressure gradient evolution occur temporarily due to blade torsional deflection mostly. Therefore, the performance obtained should be weighted by the probability of the occurrence of specific pressure gradient conditions. In practical applications of the method for wind turbine blades, moderately strong pressure gradient conditions, as demonstrated by Fritz et al. [40] for an angle of attack of 9.75 degrees, are prevalent, occurring at least 50% of the time. Therefore, selecting the WW geometry for these conditions should yield the highest performance of the method. Extreme cases, namely strong and weak APG evolutions, do not occur more than 25% of the time eachReynold. It indicates that the efficiency drop is not lower that 3.5% on average during a single cycle of torsional deflections of the blade.

In Fig. 9, the distributions of θ are presented as a function of x/δ_{in}. The results indicate the maintenance of the total momentum for the two weaker evolutions of the APG. This suggests that the higher amplitude at the end of the wavy wall, which was $A^+ = 205$ and 240 for moderately strong and weak APG evolutions, respectively, results in lower efficiency of the method but still maintains total momentum at the same level as for flat surface cases (points lying on top of each other). A properly adjusted amplitude of waviness that meets the requirement of $A^+ \approx 170$ for moderately strong APG evolution, which occurs most of the time on the wind turbine blade (50% of the time), should bring about an expected maximum increase in total momentum. To check the efficiency using Re_θ and the rest of the TBL parameters of the 13 profiles determined in the APG region, see Table 5.

Fig. 10 shows the flow field modified by the wavy wall downstream of the WW for each pressure gradient. The profiles of mean velocity and streamwise Reynolds stress were normalised by velocity at the edge of TBL U_e and are shown for all cases of pressure gradient at the location $x/\delta_{in} = 15.38$. The black symbols correspond to the flat plate case, while the open symbols represent the profiles for the WW case. In Fig. 10(a), an additional ZPG profile is shown to quantify the effect of the corrugated wall without any flow history. For the ZPG case, the increase in skin friction is 2.7%. Each graph includes the values of β for the cases with and without wall corrugation.

The mean velocity profiles collapse in the outer region and in the inner part an increase in U/U_e is observed due to the applied waviness and this effect strengthens for subsequent cases from 10(a) to 10(d). The effect of corrugation can also be observed by analysing the Reynolds stress profiles, where increased energy near the wall is

Table 5
Experimental TBL parameters for flat and wavy surfaces at different pressure gradient for $Re_{\tau,in} \approx 4000$.

x/δ_{in}	x	U_e	δ	Re_θ	Re_τ	C_f	δ^*	θ	H	u_τ
Moderate APG - Flat [41]										
7.69	0.6	21.26	96.0	17 982	4028	0.00180	18.96	13.01	1.46	0.65
10.26	0.8	20.09	116.0	21 178	4013	0.00150	26.68	16.90	1.58	0.56
12.82	1.0	18.85	129.8	23 882	3970	0.00130	33.83	20.20	1.67	0.49
15.38	1.2	17.88	152.0	28 520	4101	0.00110	48.47	25.22	1.92	0.43
Moderate APG - Wavy										
10.26	0.8	20.19	113.6	21 699	4297	0.00170	25.00	16.63	1.50	0.59
12.82	1.0	18.76	132.5	24 142	4301	0.00150	32.81	20.48	1.60	0.52
15.38	1.2	17.98	153.2	29 004	4622	0.00140	43.58	25.04	1.74	0.47
Weak APG - Flat [41]										
10.26	0.8	20.62	106.3	19 472	4089	0.00174	22.29	14.92	1.49	0.61
12.82	1.0	19.92	118.4	21 762	4265	0.00164	26.68	17.31	1.54	0.57
15.38	1.2	19.29	132.3	24 638	4453	0.00153	32.31	20.22	1.60	0.53
Weak APG - Wavy										
10.26	0.8	20.69	105.9	19 570	4245	0.00187	21.68	14.93	1.45	0.63
12.82	1.0	19.99	118.9	21 981	4516	0.00181	25.91	17.39	1.49	0.60
15.38	1.2	19.40	132.4	24 811	4779	0.00170	30.70	20.02	1.53	0.57
ZPG - flat										
15.38	1.2	19.81	94.4	13 774	4293	0.00245	13.96	10.60	1.32	0.69
ZPG - wavy										
15.38	1.2	20.05	99.2	13 772	4457	0.00254	14.24	10.93	1.30	0.72

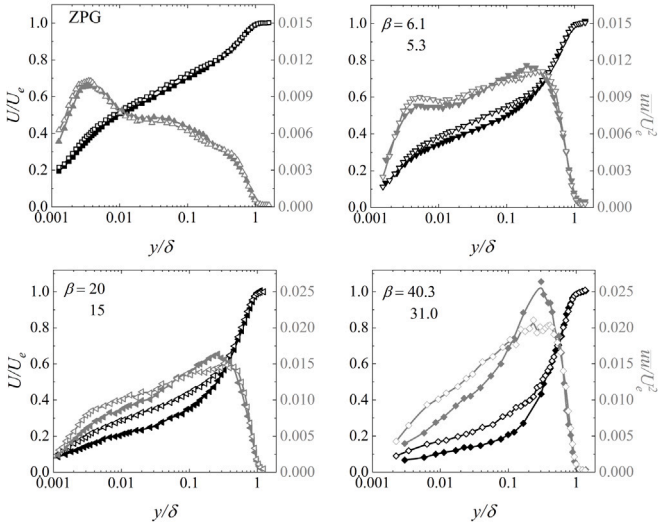

Fig. 10. Comparison of the mean velocity and velocity variance components for $x/\delta_{in} = 15.38$. ZPG flow (a), weak APG evolution (b) moderately strong APG evolution (c) and strong APG evolution (d). The star (*) indicates on-design conditions - the wavy wall adjusted to flow conditions ($A^+ = 170$).

evident. For weaker APG evolutions, the effect is less pronounced, reflecting the reduced impact of the wavy wall. As the strength of the APG increases, the observed difference becomes more significant, indicating that the method is optimised for the strongest pressure gradient conditions. This means that the effectiveness of the wavy wall in enhancing the energy near the wall is more noticeable under stronger APG conditions, while its impact diminishes with weaker APG evolutions. The change in β indicates that the wavy wall alters the flow history, weakens the effect of the pressure gradient, and postpones separation.

5. Conclusions and discussions

The study addressed the issue of near-wall flow control and the impact of streamwise corrugation on the flow separation downstream of the wavy wall under various Reynolds number and adverse pressure gradient conditions. The main goal was to confirm the universality of that method.

It has been demonstrated that the efficiency of the wavy wall was shown to decrease by no more than 2% due to the change in Reynolds number range analysed. The chosen range of Re represents the variation in inflow conditions due to the change in wind speed from 5 to 40 m/s on pitch-regulated wind turbine.

The efficiency of the method to postpone separation was also quantified by the decrease in momentum-loss thickness value. The momentum increases for $Re_\tau \approx 4000$ (as the wavy wall was implemented) and is maintained at the same level for $Re_\tau \approx 4500$. A decrease in total momentum is observed only for $Re_\tau \approx 2600$, indicating a non-optimal adaptation of the wavy wall amplitude for that Reynolds number. It has been observed that the waviness mainly affects the inner region of the boundary layer, as confirmed by the analysis of mean velocity and Reynolds stresses profiles.

The study also quantify the impact of the pressure gradient change on the performance of a wavy wall while keeping the constant Reynolds number, Such a unstable flow conditions occur on a large scale wind turbine blade due to different rotational position or torsional deflections of the blade, causing sudden changes in the inflow angle and consequently, the pressure gradient. The results show that the distribution of the pressure gradient along the surface of the airfoil and the flow history upstream play a crucial role in the performance of the flow control methods under study. However, considering the temporal nature of these changes, the average efficiency of is not lower than 3.5%. The results indicate that the selected corrugation geometry performs well under nominal and off-design operating conditions, which is particularly beneficial for offshore wind turbines.

Although 8.8% decrease in performance was observed for weak APG case, this can still be considered as a high level of effectiveness for the single geometry of surface corrugation under the impact of different pressure gradient distributions. This is due to the flow history of the pressure gradient, which causes the Reynolds stress outer peak to appear at a similar streamwise location regardless of the pressure distribution, which leads to a similar contribution of premultiplied small-scale energy to the total energy. This observation indicates that extending the wavy wall downstream of the appearance location of the outer peak in Reynolds stress will not increase the postponement of flow separation, even if the geometry of the wavy wall is adjusted to specific pressure gradient conditions.

There are also numerous other potential applications of this method in high Reynolds number aero and hydrodynamic systems where flow

separation control is crucial. These include fast trains, missiles, trucks, ships, and more.

The future study will examine the performance of the wavy wall applied to a curved surface resembling a blade surface. Additionally, there are plans to modify the geometry of the corrugation by altering the tilt of the wave and introducing a non-harmonic wave type.

CRediT authorship contribution statement

Artur Dróżdż: Writing – review & editing, Writing – original draft, Visualization, Validation, Supervision, Software, Resources, Methodology, Investigation, Formal analysis, Data curation, Conceptualization. **Vasyl Sokolenko:** Methodology, Investigation. **Witold Elsner:** Writing – review & editing, Supervision, Resources, Project administration, Investigation, Funding acquisition, Formal analysis, Conceptualization,Validation.

Declaration of competing interest

The authors declare that they have no known competing financial interests or personal relationships that could have appeared to influence the work reported in this paper.

Acknowledgements

The investigation was supported by National Science Centre, Poland under Grant No. DEC-2020/39/B/ST8/01449.

Data availability

Data and procedure mentioned in this study can be found at Repository for Open Data - RepOD: https://doi.org/10.18150/FTHEI6.

References

[1] Mohammad Hassan Shojaeefard, Salman Saremian, Analyzing the impact of blade geometrical parameters on energy recovery and efficiency of centrifugal pump as turbine installed in the pressure-reducing station, Energy 289 (2024) 130004.
[2] Duc Anh Nguyen, Jin Hyuk Kim, Co-adjustable guide vane and diffuser vane to improve the energy generation potential of an axial-flow pump as turbine, Energy 291 (2024) 130325.
[3] Ph. Devinant, T. Laverne, J. Hureau, Experimental study of wind-turbine airfoil aerodynamics in high turbulence, J. Wind Eng. Ind. Aerodyn. 90 (6) (2002) 689–707.
[4] Wenyao Cui, Zhixiang Xiao, Xiangjiang Yuan, Simulations of transition and separation past a wind-turbine airfoil near stall, Energy 205 (2020) 118003.
[5] Abolfazl Abdolahifar, S.M.H. Karimian, A comprehensive three-dimensional study on Darrieus vertical axis wind turbine with slotted blade to reduce flow separation, Energy 248 (2022) 123632.
[6] He Yong Xu, Chen Liang Qiao, Hui Qiang Yang, Zheng Yin Ye, Delayed detached eddy simulation of the wind turbine airfoil S809 for angles of attack up to 90 degrees, Energy 118 (2017) 1090–1109.
[7] Ying Wang, Gaohui Li, Sheng Shen, Diangui Huang, Zhongquan Zheng, Influence of an off-surface small structure on the flow control effect on horizontal axis wind turbine at different relative inflow angles, Energy 160 (2018) 101–121.
[8] F. Azlan, M.K. Tan, B.T. Tan, M.Z. Ismadi, Passive flow-field control using dimples for performance enhancement of horizontal axis wind turbine, Energy 271 (2023) 127090.
[9] Juliana de Almeida Yanaguizawa Lucena, Recent advances and technology trends of wind turbines, in: Recent Advances in Renewable Energy Technologies: Volume 1, 2021, pp. 177–210.
[10] Masaru Koike, Tsunehisa Nagayoshi, Naoki Hamamoto, Research on aerodynamic drag reduction by vortex generators, Mitsubishi Mot. Tech. Rev. 16 (2004) 11–16.
[11] Jean-Luc Aider, Jean-François Beaudoin, José Eduardo Wesfreid, Drag and lift reduction of a 3d bluff-body using active vortex generators, Exp. Fluids 48 (2010) 771–789.
[12] Pedro D. Bravo-Mosquera, Fernando M. Catalano, David W. Zingg, Unconventional aircraft for civil aviation: A review of concepts and design methodologies, Prog. Aerosp. Sci. 131 (2021) 2022.
[13] John H. McMasters, Michael L. Henderson, Low-speed single-element airfoil synthesis, in: NASA. Langley Res. Center the Sci. and Technol. of Low Speed and Motorless Flight, Pt. 1, 1979.
[14] Pierre Ricco, Martin Skote, Michael A. Leschziner, A review of turbulent skin-friction drag reduction by near-wall transverse forcing, Prog. Aerosp. Sci. 123 (2021) 100713.
[15] Jin Choi, Woo-Pyung Jeon, Haecheon Choi, Mechanism of drag reduction by dimples on a sphere, Phys. Fluids 18 (4) (2006) 1.
[16] C.M.J. Tay, B.C. Khoo, Y.T. Chew, Mechanics of drag reduction by shallow dimples in channel flow, Phys. Fluids 27 (3) (2015) 1.
[17] Federica Gattere, Alessandro Chiarini, Maurizio Quadrio, Dimples for skin-friction drag reduction: status and perspectives, Fluids 7 (7) (2022) 240.
[18] Katsumi Aoki, Koji Muto, Hiroo Okanaga, Mechanism of drag reduction by dimple structures on a sphere, J. Fluid Sci. Technol. 7 (1) (2012) 1–10.
[19] Peter W. Bearman, John K. Harvey, Golf ball aerodynamics, Aeronaut. Q. 27 (2) (1976) 112–122.
[20] C. Tay, Determining the effect of dimples on drag in a turbulent channel flow, in: 49th AIAA Aerospace Sciences Meeting Including the New Horizons Forum and Aerospace Exposition, 2011, p. 682.
[21] Seong-Ho Seo, Cheol-Hyun Hong, Performance improvement of airfoils for wind blade with the groove, Int. J. Green Energy 13 (1) (2016) 34–39.
[22] Riyadh Belamadi, Abdelouaheb Djemili, Adrian Ilinca, Ramzi Mdouki, Aerodynamic performance analysis of slotted airfoils for application to wind turbine blades, J. Wind Eng. Ind. Aerodyn. 151 (2016) 79–99.
[23] James G. Coder, Dan M. Somers, Design of a slotted, natural-laminar-flow airfoil for commercial transport applications, Aerosp. Sci. Technol. 106 (2020) 106217.
[24] Wafaa Mostafa, Abouelmagd Abdelsamie, Momtaz Sedrak, Dominique Thévenin, Mohamed H. Mohamed, Quantitative impact of a micro-cylinder as a passive flow control on a horizontal axis wind turbine performance, Energy 244 (2022) 122654.
[25] Jiang-Sheng Wang, Jun Wu, Jin-Jun Wang, Wake-triggered secondary vortices over a cylinder/airfoil configuration, Exp. Fluids 64 (1) (2023) 6.
[26] A. Dróżdż, P. Niegodajew, M. Romańczyk, V. Sokolenko, W. Elsner, Effective use of the streamwise waviness in the control of turbulent separation, Exp. Therm. Fluid Sci. 121 (2021) 110291.
[27] A. Dróżdż, W. Elsner, D. Sikorski, Passive skin friction control near turbulent separation–preliminary results, in: Journal of Physics: Conference Series, Vol. 1101, IOP Publishing, 2018, 012004.
[28] W. Elsner, A. Dróżdż, E. Szymanek, A. Tyliszczak, P. Niegodajew, Experimental and numerical studies of turbulent flows over two-dimensional and three-dimensional rough surfaces under an adverse pressure gradient, Appl. Math. Model. 106 (2022) 549–566.
[29] P. Kamiński, P. Niegodajew, A. Drózdz, V. Sokolenko, A. Tyliszczak, W. Elsner, Numerical analysis of novel wavy wall based control of turbulent boundary layer separation, Aerosp. Sci. Technol. 149 (2024) 109167.
[30] Romain Mathis, Jason P. Monty, Nicholas Hutchins, Ivan Marusic, Comparison of large-scale amplitude modulation in turbulent boundary layers, pipes, and channel flows, Phys. Fluids 21 (11) (2009) 111703.
[31] A. Dróżdż, P. Niegodajew, M. Romańczyk, W. Elsner, Convection velocity in turbulent boundary layers under adverse pressure gradient, Exp. Therm. Fluid Sci. (2023) 110900.
[32] Tianshu Liu, Tao Chen, Massimo Miozzi, Correlation between skin friction and enstrophy convection velocity in near-wall turbulence, Eur. J. Mech. B Fluids 104 (2024) 224–230.
[33] N. Agastya Balantrapu, Christopher Hickling, W. Nathan Alexander, William Devenport, The structure of a highly decelerated axisymmetric turbulent boundary layer, J. Fluid Mech. 929 (A9) (2021) 1–38.
[34] Mohamed A. Sayed, Hamdy A. Kandil, El-Sayed I. Morgan, Computational fluid dynamics study of wind turbine blade profiles at low reynolds numbers for various angles of attack, AIP Conf. Proc. 1440 (2012) 467–479, Cited by: 3.
[35] A. Dróżdż, P. Niegodajew, M. Romańczyk, W. Elsner, Effect of reynolds number on turbulent boundary layer approaching separation, Exp. Therm. Fluid Sci. 125 (2021) 110377.
[36] P. Niegodajew, A. Drózdz, W. Elsner, A new approach for estimation of the skin friction in turbulent boundary layer under the adverse pressure gradient conditions, Int. J. Heat Fluid Flow 79 (2019) 108456.
[37] A. Dróżdż, R. Örlü, V. Sokolenko, P. Schlatter, W. Elsner, P. Niegodajew, Hot-wire spatial resolution issues in adverse pressure gradient turbulent boundary layers, Meas. 237 (2024) 115229.
[38] Ricardo Vinuesa, Seyed M. Hosseini, Ardeshir Hanifi, Dan S. Henningson, Philipp Schlatter, Pressure-gradient turbulent boundary layers developing around a wing section, Flow Turbul. Combust. 99 (2017) 613–641.
[39] A. Bobke, R. Vinuesa, R. Örlü, P. Schlatter, History effects and near equilibrium in adverse-pressure-gradient turbulent boundary layers, J. Fluid Mech. 820 (2017) 667–692.
[40] E.K. Fritz, C.L. Kelley, K.A. Brown, On optimizing the sensor spacing for pressure measurements on wind turbine airfoils, Wind. Energy Sci. 9 (8) (2024) 1713–1726.
[41] A. Drózdz, P. Niegodajew, W. Elsner, R. Örlü, V. Sokolenko, P. Schlatter, Data for publication: Hot-wire spatial resolution issues in adverse pressure gradient turbulent boundary layers, 2024.